# MASTERARBEIT | MASTER'S THESIS

Titel | Title

"Single cell activity of major bacterial groups in the surface microlayer of a mesocosm during an induced phytoplankton bloom."

verfasst von | submitted by

Sarah Joy Bowen

angestrebter akademischer Grad | in partial fulfilment of the requirements for the degree of

Master of Science (MSc)

Wien | Vienna, 2025

| | |
|---|---|
| Studienkennzahl lt. Studienblatt \| Degree programme code as it appears on the student record sheet: | UA 066 833 |
| Studienrichtung lt. Studienblatt \| Degree programme as it appears on the student record sheet: | Masterstudium Ecology and Ecosystems |
| Betreut von \| Supervisor: | Mag. Dr. Thomas Reinthaler |

## Zusammenfassung

Da die Luft- und Meerestemperaturen durch den rasanten Anstieg der globalen CO2-Emissionen weiter steigen, umso signifikanter wird es, die Mechanismen zu verstehen, die für die Kohlenstoff- und Temperaturschwankungen an der Grenzfläche zwischen Luft und Meer verantwortlich sind. Die Mikroschicht der Meeresoberfläche (SML) ist ein einzigartiger Lebensraum an dieser Grenzfläche, welche für die Abschätzung des Gasaustauschs zwischen Luft und Meer von unschätzbarem Wert ist. Heterotrophe Bakterien in dieser Umgebung unterscheiden sich nachweislich vom darunter liegenden Wasser (ULW), und angesichts ihrer bedeutenden Rolle beim Recycling organischer Stoffe sind genaue Schätzungen ihrer Aktivität im Vergleich zur Atmung von entscheidender Bedeutung für die Vorhersage von CO2-Übersättigung und Ausgasung aus dem Meer. Es ist bekannt, dass Algenblüten verschiedene Auswirkungen auf unterschiedliche Bakteriengruppen haben, doch wie sie sich auf die Bakterien in der SML auswirken, ist gegenwärtig noch nicht geklärt. In dieser Studie wurde die Sukzession der Bakteriengruppen nach den Veränderungen der Algendominanz während einer simulierten Phytoplanktonblüte in einem Mesokosmos verfolgt. Mit Hilfe von Fluoreszenz-in-situ-Hybridisierung (FISH) und Homopropargylglycin (HPG)-Assimilation unter Verwendung von Click-Chemie wurden die Zellhäufigkeit, wie auch Zellaktivität verschiedener Bakteriengruppen, insbesondere Bacteroidetes, Roseobacter und SAR11, bestimmt. Während der zweiten und dritten Phase der Algenblüte wurde ein statistischer Unterschied in der Abundanz und Aktivität zwischen dem SML und dem ULW festgestellt. SAR11 im SML und ULW wies während der verschiedenen Blütephasen Spitzenwerte in Häufigkeit und Aktivität auf, was darauf hindeutet, dass in jeder Schicht unterschiedliche Mitglieder dieser Bakteriengruppe vorhanden sind. Die DOC-Konzentrationen wiesen die stärksten Korrelationen mit SAR11 auf, und Unterschiede in der DOC-Zusammensetzung sind wahrscheinlich für das unterschiedliche Verhalten innerhalb der einzelnen Schichten in Reaktion auf die Blüte verantwortlich.

## Abstract

As air and sea temperatures continue to increase from the rise in global $CO_2$ emissions, understanding the mechanisms responsible for carbon and temperature fluctuations at the air-sea interface is increasingly important. The sea surface microlayer (SML) is a unique habitat that exists at this interface, rendering it invaluable for estimating air-sea gas exchanges. Heterotrophic bacteria in this environment have proven to be distinct from the underlying water (ULW) beneath, and given their significant role in the recycling of organic matter accurate estimations in their activity vs. respiration is crucial for predicting $CO_2$ supersaturation and outgassing from the sea. Algal blooms are known to have various effects on different bacterial groups, however, how they affect bacteria in the SML is yet to be determined. This study tracked the succession of bacterial groups following the changes in algal dominance during a simulated phytoplankton bloom in a mesocosm. Fluorescence in-situ hybridization (FISH) and Homopropargylglycine (HPG) assimilation using Click-chemistry were used to determine the single-cell abundance and activity of various bacterial groups, particularly Bacteroidetes, Roseobacter, and SAR11. A comparative analysis of these bacterial groups within the SML and ULW was conducted throughout three phases of the algal bloom while also incorporating environmental measurements for insights into their influence on the microbial abundance and activity. During the second and third phases of the algal bloom a statistical difference in the abundance and activity between the SML and ULW was observed. SAR11 in the SML and ULW showed peaks of abundance and activity during different bloom phases, suggesting different members of this bacterial group are present within each layer. DOC concentrations showed the strongest correlations with SAR11 and differences in the DOC composition are likely responsible for the differing behavior within each layer in response to the bloom.

**Keywords: North Sea, sea surface microlayer, fluorescence in-situ hybridization, Homopropargylglycine (HPG) assimilation, marine phytoplankton bloom, heterotrophic bacteria**

## Acknowledgements

I would first and foremost like to thank my thesis supervisor Mag. Dr. Thomas Reinthaler for his continued guidance and support throughout this project. His helpful feedback and enthusiasm for my ideas and work contributed to the success of my thesis. Additionally, his lectures were some of my favorites throughout this degree program and laid a great foundation for knowledge required for this project.

I would also like to thank PhD candidate, Dmytro Spriahailo, who endured countless questions from me on all things lab and R related, no matter how trivial. I would not have finished without his continued help and am grateful for his always positive attitude.

PhD Chie Amano is responsible for imparting her extensive knowledge in the ways of FISH and Click-chemistry analysis, as well as fluorescence microscopy, all of which are the foundations of the lab work on the project, and I owe her many thanks for her patience and willingness to teach me.

A special thanks goes to my fellow master's student Vera Hechtl, who has become a close friend during this process as well as an important listener and collaborator on our parallel projects.

Finally, I would like to thank my partner Kaveh Siah, for his continued support of my studies and education, from when we lived on separate continents, to joining me in Vienna, and even offering his own insight to this project until the very end.

# Table of Contents

## *Introduction*

Atmospheric $CO_2$ concentrations strongly correlate to anthropogenic carbon emissions and are expected to continue to rise in the next century. Increasing $CO_2$ concentrations result in higher surface temperatures around the globe, with a current anomaly of 0.2°C of warming per decade, defined by the IPCC as an increase in global averaged sea and air surface temperatures since pre-industrial levels (IPCC, 2022, Samset et al. 2020). As the world's oceans function as a sink for both atmospheric $CO_2$ and heat, it is critical to understand the mechanisms under which these take place to accurately predict the future outcomes we can expect on a warming planet. The sea surface microlayer (SML) is a unique habitat that exists as the boundary layer between the atmosphere and the sea (Reinthaler et al. 2008; Wurl et al. 2017) and harbors a microbial community distinct from the underlying water (ULW) (Franklin et al. 2005; Wurl et al. 2011). The bacteria residing in this boundary layer, referred to as bacterioneuston, play a key role in the recycling of organic matter and possibly control part of the flux of anthropogenic trace gases such as $CO_2$. Previous work by Obernosterer et al. (2005) on the effect of carbon cycling within the SML and the importance of bacterial metabolic activity showed that community respiration rates were higher in the SML compared to the ULW. Additionally, primary production in the SML was not sufficient to support respiration rates, suggesting that vertical transport of organic matter from the ULW compensated for this discrepancy. The higher respiration rates in the SML also contributed to increased dissolved inorganic carbon (DIC) at the boundary layer, affecting the air-sea gas exchange (Obernosterer et al. 2005). More specifically, when net heterotrophic metabolism is less than respiration this may lead to $CO_2$ supersaturation in the top centimeters of ocean, resulting in outgassing of $CO_2$ to the atmosphere (Calleja et al. 2005).

Understanding bacterial metabolic activity is integral for understanding organic matter cycling because bacteria are responsible for the remineralization of dissolved organic matter (DOM) that largely stems from primary production by phytoplankton in the surface ocean. Heterotrophic bacteria assimilate organic matter and use it for biomass production and respiration, the latter resulting in $CO_2$ production. The biomass is grazed upon by protists and microzooplankton while the $CO_2$ enters the inorganic carbon cycle and can be taken up by photoautotrophs or exchanged with the atmosphere, thus reentering the atmosphere as a greenhouse gas (del Giorgio and Cole 1998).

Labile dissolved organic matter (DOM) in the surface is provided by phytoplankton via the excretion of exudates, viral lysis, and sloppy feeding by zooplankton (Lancelot and Billen 1984; Alderkamp et al. 2006). The labile DOM generally leads to higher abundances and activity of bacteria and archaea (Alderkamp et al. 2006; Wemheuer et al. 2015), however, not all

phytoplankton blooms affect bacterial groups equally. Several studies have found that various environmental and biotic factors affect which bacterial groups benefit from bloom conditions. A common conclusion from these studies investigating the interactions of phytoplankton and bacteria as well as organic matter composition, is that the dominance of specific bacterial groups changes in succession with the changing substrate released by the blooms (Rink et al. 2007; Reintjes et al. 2020; Brüwer et al. 2023). Furthermore, these studies suggest that phytoplankton blooms provide specific ecological niches that are filled by a few bacterial groups, rather than leading to a general increase in total community abundance and activity (Wemheuer et al. 2014; Bakenhus et al. 2017). E.g., Roseobacter and Flavobacteria seem to benefit the most from high molecular weight (HMW) organic matter that is produced during and after blooms (Rink et al. 2007; Wemheuer et al. 2014), particularly, complex organic matter such as polysaccharides, chitin and algal proteins (Alderkamp et al. 2006; Wemheuer et al. 2015). Thus, identifying the bacterial community associated with the phytoplankton in the SML will provide insight into the ecological distinctions between the SML and ULW.

Despite the potentially large significance of the SML as the boundary layer of sea, few studies have investigated the microbial communities of this specific habitat, and conflicting reports as to whether a difference in bacterial composition between the SML and ULW exists, have been reported (Franklin et al. 2005; Agogué et al. 2005; Obernosterer et al. 2008). According to Franklin et al. (2005), the SML was found to contain bacterial populations that were distinct but significantly less diverse from the ULW and hosted different dominating bacterial taxa. Agogué et al. (2005) also found distinct bacterial strains present in the SML, but no difference between the dominating species of each layer. Obernosterer et al. (2008) reported >76% similarity of the bacterial composition between the layers as well as lower bacterial production in the SML. Among the few studies measuring respiration in the SML, higher rates were reported in the SML compared to the ULW (Obernosterer et al. 2005; Reinthaler et al. 2008). The concentrations and accessibility of organic matter in the SML was found to be insufficient to support the respiration rates, concluding that physical transport from the ULW made up for the discrepancy (Franklin et al. 2005; Reinthaler et al. 2008). While the relationship between bacteria and phytoplankton blooms has been investigated in the sunlit surface ocean, and bacterial communities and their metabolic activity have been explored to an extent, the relationship of bacterial communities with phytoplankton blooming in the SML has yet to be established.

We investigated the development of an artificially initiated phytoplankton bloom and the paralleled succession of bacterial groups during a mesocosm experiment. We hypothesized that

metabolic activity is lower in the SML compared to the ULW during non-bloom conditions due to effects of UV radiation on bacterial activity (Herndl 1993) as well as organic matter availability in the SML. UV radiation can cause refractory DOM to become more labile and vice versa. Depending on the type of UV radiation (UVA or UVB), the amount of labile versus recalcitrant DOM can change according to the intensity and exposure time of the two radiation types, thus affecting the amount of DOM available to bacteria. UV radiation can also directly affect bacterial activity, depending on the type of radiation. UVB radiation causes DNA damage in the bacterial cells, inhibiting their activity, while UVA radiation can reverse this damage, allowing for the bacterial assimilation of DOM (Winter et al. 2001). As the SML has more direct exposure to UV radiation compared to the ULW, it follows that any detrimental effects such as UVB-caused DNA damage would be more severe in the SML. The increase of fresh organic matter provided by the phytoplankton during the bloom, however, might counteract any DNA damage and significantly enhance the metabolic activity in the SML. Thus, we compared the SML and ULW with regard to the growth dynamics of specific bacterial groups during the development of the phytoplankton bloom and also assessed the influence of environmental parameters on the microbial activity.

## *Methods*

### Mesocosm and experimental setup

To quantify the influences of a phytoplankton bloom on bacterial activity in the SML, a mesocosm experiment was conducted in the Sea Surface Facility (SURF) at the ICBM Wilhelmshaven, Germany, from May - June 2023 (**Fig. 1**). In the 32-day experiment a phytoplankton bloom of Prymnesiales indet. of the class *Coccolithophyceae* was promoted by nutrient additions of sodium metasilicate nonahydrate ($Na_2O_2Si.9H_2O$), sodium nitrate ($NaNO_3^-$), and sodium dihydrogen phosphate ($Na_2HPO_4$) on days 11, 16, and 17 of the experiment. Bacterial samples were collected from the SML and ULW every third day, starting on 16 May, and ending on 15 June.

**Figure 1.** The Sea Surface Facility (SURF) at ICBM Wilhelmshaven, Germany includes a basin, a retractable roof, and several on-site instruments to control some water parameters and to monitor the physical parameters (see text for a detailed description).

## Environmental parameters

Water temperature was measured at a depth of < 2 cm using a Unisense PT 1000 temperature Sensor. Salinity and pH measurements were taken from two Sea and Sun CTDs from both the SML as close to water surface as possible, and the ULW sampled at 40 cm. Chlorophyll-a measurements were taken using a FerryBox fluorometer mounted on the Bio-Optical Sensor Package (BOP) at 30 – 40 cm depth. Blank measurements using MilliQ were taken with all sensors before and after the experiment to check for instrument shifts. Blank measurement shifts were subtracted from the measured chlorophyll-a data. Due to photochemical quenching the fluorometric measurements were not accurate during the day as the presence of sunlight interfered with the fluorometer's ability to accurately detect the chlorophyll fluorescence emitted from the algae (Murchie and Lawson 2013). This data gap was filled with in-situ absorbance data collected using a spectral absorption sensor (ac-s Spectral Absorption and Attenuation Sensor, Seabird Scientific). Absorbances were converted to chlorophyll-a concentrations and then scaled to daily HPLC measurements using the method from Collin and Barnard (2013). Irradiation was measured with a radiometer secured to a pole in the mesocosm and recorded downward irradiance of wavelengths between 319 nm and 953 nm (Pyranometer SR20-D2, Hukseflux). All the online sensor measurements were averaged over a day.

Particulate organic carbon (POC) concentrations were measured from samples taken from the ULW using an elemental analyzer (EURO EA). Blanks were subtracted from the raw data after which the average of all replicates was taken for each day (Sharp, 1974). Dissolved organic carbon (DOC) samples were prepared using sequential filtration over 5.0, 3.0, and 0.2 µm

polycarbonate filters (Whatman, Nuclepore) and measured using the high temperature combustion method on a Shimadzu TOC-VCPH analyzer. Certified deep sea reference material (D.A. Hansell, University of Miami, FL, USA) was used for calibration. Dissolved inorganic carbon (DIC) measurements were measured using the coulometric titration method (Dickson et al., 2007). Inorganic nutrients were measured using a continuous flow analyzer after samples were filtered with a 0.45 µm SFCA syringe filters and poisoned with mercury, following the protocol of Doane et al. (2003). A sequential automatic analyzer (Easychem, Systea S.p. Italy) was used to analyze nitrite ($NO_2^-$), nitrate ($NO_3^-$), phosphate ($PO_4^{-3}$), and silicate (Si) with the respective detection limits: 0.4 µM, 0.4 µM, 0.04 µM, and 0.1 µM, and limits of determination of 1.0, 0.13, and 0.4 µM.

**Biological measurements**

For bacterial measurements, the glass plate method was used in the SML (Harvey and Burzell 1972) in which a glass plate of dimensions 50 cm long by 25 cm wide was dipped vertically into the surface of the mesocosm, penetrating the accumulated SML as well as the water below. After retracting the plate and waiting 20 s for all excess water to drip off, the remaining film from the SML was scraped into a flask, the average final volume resulting in 500 mL. All glassware was cleaned with HCl between samplings. The ULW was sampled using a plastic bottle at a depth of 40 cm. Immediately after collection, samples were prefiltered using 5 µm pore size polycarbonate filters. In subsamples cells were stained with SYBR Green and checked under a fluorescence microscope to determine a sampling volume that resulted in approximately 100 cells per field of view. The appropriate volumes for each sampled time point were then incubated using the methodology described in more detail below for BONCAT, RSG and FISH analyses. After incubation, the samples were filtered onto 0.2 µm polycarbonate filters (Millipore GTTP, 25 mm diameter) and immediately frozen at -20°C for storage. These bacterial samples were collected from 11 timepoints throughout the 32-day experiment (every third day). From these 11 samples, 5 were chosen to represent each stage of the bloom, culminating in the samples from days 1, 13, 19, 25, and 31 being used for further analysis with FISH and Click-chemistry. Additional samples were stored at -20°C after filtering for later counting with a flow cytometer following the method from Brussaard et al. (2010). Phytoplankton cells were collected from the ULW, preserved in Lugol and abundances were determined using inverted microscopy.

**Biomass production via bioorthogonal non-canonical amino acid tagging (BONCAT)**

The number of active bacterial cells was estimated with assimilation assays of Homopropargylglycine (HPG) in which a fluorophore is attached to the methionine analogue using Click-chemistry. In conjunction with FISH analysis, this approach allows to estimate single-cell biomass production of specific bacterial groups (Leizeaga et al. 2017).

Between 120-800 µL of HPG solution (Click-iT Protein Enrichment Kit, ThermoFischer) was added to duplicate samples from both the SML and ULW at each sampling timepoint to reach a final concentration of 20 nM. All samples were then incubated in the dark at room temperature for 4 hours, fixed with 35% sterile-filtered formaldehyde and filtered onto 0.2 µm polycarbonate filters (Millipore GTTP, 25 mm diameter). Subsequently, filters were stored at -20°C until further analysis. Back in the lab the filters were incubated with a reaction buffer containing Alexa647 (ThermoFisher Scientific), Click-iT HPG reaction 10x concentration (ThermoFisher Scientific), copper solution, a buffer additive, and Sigma Water in a microfuge tube at room temperature in the dark for 30 minutes. Filters were washed with Milli-Q and dried at 37°C in a hybridization oven for 10 minutes before an embedding step (see FISH protocol below). After the BONCAT procedure the filters were further stored at -20°C until FISH processing (see below).

**Respiration via Redox Sensor Green (RSG)**

For single-cell respiration estimates several samples were spiked directly after sampling with RSG stock solution, to reach a final concentration of 1 µM. Samples were incubated in the dark for 30 minutes at in situ temperature and bacterial activity was terminated with 35% sterile-filtered formaldehyde. The seawater was filtered onto 0.2 µm polycarbonate filters (Millipore GTTP, 25 mm diameter) and immediately frozen at -20°C for later analyses in the lab. All filters containing RSG were to be directly subjected to the FISH protocol. The published RSG protocol we used (Munson-McGee et al. 2002) was incomplete and fixation with formaldehyde produced autofluorescence that even after adjustments and intensive testing did not produce reliable results. Consequently, the filters containing RSG were not used in the final analysis of this study (see discussion).

**Fluorescence in-situ hybridization of specific microbial groups (FISH)**

Fluorescence in-situ hybridization (FISH) was used to detect major bacterial groups in the SML and the ULW (Amann et al. 1995). To prevent the loss of cells we embedded the filters after the Click-chemistry procedure using a 0.1% low-melting point agarose solution that was heated to 35°C to reach the desired viscosity for embedding. The agarose-coated filters were first air-

dried for 15 minutes and then dried in a hybridization oven at 37°C. Depending on the probe employed, a hybridization buffer with formamide concentrations between 20–50% was used (see **Table 1**). To a microfuge tube, 297 µL of buffer consisting of 5M NaCl, 1M Tris-HCl, Dextran Sulfate, 100% Triton x100, formamide, 10% Blocking, and Sigma Water, plus 3 µL of a fluorescently labeled probe (Biomers) was added and gently mixed. Into the buffer/probe solution a 1/12 section of filter from all chosen timepoints was added. The tubes were hybridized in an oven set to 46°C and rotated for 3 hours. After hybridization, the filter sections were transferred to a 50 mL Falcon tube containing a washing buffer (80 mM NaCl, 20 mM Tris/HCl, 5 mM EDTA and MilliQ water) and placed in a water bath at 48°C for 15 minutes. All filter sections were mounted on 1 mm microscope slides using a DAPI mix containing DAPI (2 µg $mL^{-1}$), 1x PBS (0.5 µg $mL^{-1}$), Vectashield (1 µg $mL^{-1}$), and Citifluor (5.5 µg $mL^{-1}$) for counterstaining of total bacterial abundance.

A total of seven bacterial probes plus a positive and negative control (see **Table 1** below) were selected for FISH. The choice of probes was based on previous studies conducted during phytoplankton blooms in the North Sea, as well as a study conducted with mesocosms (see discussion). Of the seven probes, Alphaproteobacteria, Roseobacter, SAR11, and Bacteroidetes (Bacteroidetes, Flavobacteria, Sphingobacteria) were selected for our final analysis. Selection was based on preliminary testing of all seven probes in which FISH and Click were performed on samples from the beginning, the middle, and the end of the bloom. The bacterial groups not selected reached less than 1.5% of the total community on a filtered sample. To verify that the total abundance of bacteria (counted in the DAPI channel) were accurate a filter section from the first time point and each layer was mounted with the DAPI mix without FISH treatment.

**Table 1.** FISH probe sequences, formamide concentrations used in the buffer and authors.

| Target group | Probe | Sequence | %Formamide | Author |
|---|---|---|---|---|
| Bacteria | EUB338 I | GCTGCCTCCCGTAGGAG | 0-50 | Amann et al. 1990 |
| | EUB338 II | GCAGCCACCCGTAGGTGT | | Daims et al. 1999 |
| | EUB338 III | GCTGCCACCCGTAGGTGT | | Daims et al. 1999 |
| None | NON-EUB | ACTCCTACGGGAGGCAGC | | Wallner et al. 1993 |
| Alphaproteobacteria | ALF968 | TGGTAAGGTTCTGCGCGT | 20 | Manz et al. 1992 |
| Alteromonas | Alt1413 | TTTGCATCCCACTCCCAT | 40 | Eilers et al. 2000 |
| Flavobacteria, Bacteroidetes, Sphingobacteria | Bacteroidetes | TGGTCCGTGTCTCAre TAC | 35 | Manz et al. 2000 |
| Gammaproteobacteria | GAM42a | GCCTTCCCACATCGTTT | 35 | Manz et al. 1992 |
| Roseobacteraceae + competitor | Roseo536R<br>RoseoC536R | CAACGCTAACCCCCTCCG<br>CAACGCTAGCCCCCTCCG | 40 | Tolli et al. 2006 |
| Pelagibacteraceae SAR11 | SAR11-441R | TACAGTCATTTTCTTCCCCGAC | 45 | Morris et al. 2002 |
| Verrucomicrobia | VP403 | CGAAGACCTTATCCTCCA CG | 35 | Arnds et al. 2010 |

**Fluorescent microscopy**

The DAPI-mounted filter pieces were analyzed with a ZEISS Axio Imager 2 epifluorescence microscope, using the filter sets: DAPI, FITC, Cy3, and Cy5. Cells in the DAPI channel (Ex/Em: 368/461 nm) fluoresced blue and yielded the total abundance of cells containing DNA. RSG (Ex/Em: 495/519 nm) fluoresced green and showed cells actively respiring, using the FITC channel. Cells in the Cy3 channel (Ex/Em: 554/566 nm) fluoresced orange and showed cells hybridized to a FISH probe. Alexa647 (Ex/Em: 650/671 nm) fluoresced red under the Cy5 filter set, revealing translationally active cells. To avoid false positive fluorescent signals stemming from crossover between the FITC, Cy3, and Cy5 channels, RSG samples were assayed separately from those containing HPG. Ten photos per channel were taken in a grid of 0.5 mm increments for each filter section, targeting the midsection of the filter where cells were most likely to be evenly distributed.

A total of 600 photos was generated and analyzed with the ACME software tool (Bennke et al. 2016), which allowed for automated counting of cells and comparison between fluorescent channels. Photos were preselected in ACME to exclude any poor-quality images, and all remaining images were compiled into a metafile for further processing. Cells were counted in each image if they fit the criteria set under the following variables: cell area (pixels), surface-to-background ratio (SBR), MGV, elongation, and length (pixels). This ensured that only bacterial cells were counted while particles, probe aggregates, and large organisms such as phytoplankton cells, were excluded. Depending on the quality of the image, various combinations of the variables were used, with the variables ranging as follows: SBR = 1.1–1.7, cell area = 6–650, MGV = 30–50, elongation <15, and length <35. Each photo was manually selected for batches of parameters with the best fit. When it was not possible to count all bacterial cells by adjusting the parameters alone, cells were manually marked using the marker function and labeled according to the appropriate cell type. When probe deposits, unspecific binding, or larger cells were analyzed as many smaller cells, a marker was also used to exclude false positives. Sample reports were generated in ACME and all marker counts added to their respective categories, yielding more accurate results. The raw abundance data from each channel of the non-EUB probe was subtracted from the overlapping abundance data (cells detected in both the DAPI and Cy3 channel for FISH and the DAPI and Cy5 for Click), to establish the amount of probe deposits detected in each sample. For FISH abundances the cells detected in the Cy3 channel without using the overlap feature were used to detect cells in each bacterial group. For Click abundances all cells in the Cy5 channel that overlapped with cells in the Cy3 channel were used to determine the number of active cells in each bacterial group. For

each sample (date and sample depth), the probe deposits were subtracted from each probe's raw abundance data. The following formula was used to calculate the absolute abundance for each probe and sample:

$$Abundance\ (cells\ mL^{-1}) = \frac{\frac{(raw\ abundance - NonEUB\ counts)}{number\ of\ FOVs}}{FOV\ area\ (\mu m^2)} \times \frac{area\ of\ sample\ (\mu m^2)}{filtered\ sample\ volume\ (mL)}$$

Raw abundance refers to the raw bacterial counts of a single probe, and the non-EUB probe deposits were determined by counting all signals in the respective Cy3 and Cy5 channels that could not be attributed to fluorescence from larger organisms bleeding into these channels from the DAPI channel. FOV refers to the field of view of each photo, the number of FOVs refers to the number of photos taken for each sample. The FOV area is the frame size used to analyze the photos in ACME. The area of sample is the size of the filtration funnel used when filtering the samples, so the total area of the filter covered in sample. Filtered sample volume is the amount of sample filtered in mL.

**Statistical analysis**

The final analyses, graphs and statistics were conducted in R (Version 4.4.2). Nonparametric tests were used to test for differences in bacterial abundance and activity between the SML and ULW. Tracking the changes and characteristics in bacterial growth was done with the Growthcurver (Version 0.3.1) function in R by fitting the growth data to a standard logistic growth curve. General correlations between bacteria and environmental parameters were calculated using the Spearman's rank test. A more detailed analysis was conducted with redundancy analysis after Hellinger transformations of the abundance and activity data as well as z-score transformations of the environmental variables. Packages used included ape (Version 5.8), Cairo (Version 1.6.2), coin (Version 1.4.3), corrplot (Version 0.94), datarium (Version 0.1.0), extraoperators (Version 0.3.0), Hmisc (Version 5.1.3), Jwileymisc (Version 1.4.1), lattice (Version 0.22.5), rstatix (Version 0.7.2), tidyverse (Version 2.0.0), and vegan (Version 2.6.6.1).

## *Results*

**Environmental parameters**

The daily irradiance measurements fluctuated throughout the experiment with a minimum

value of 1.9 ×$10^7$ W $m^{-2}$ × $day^{-1}$ and a maximum of 9.3 × $10^7$ W $m^{-2}$ $day^{-1}$. From day 18 until the end of the experiment the irradiance varied around the maximum within a narrow range of 6.2 to 9.3 × $10^7$ W $m^{-2}$ $day^{-1}$ (**Fig. 2a**). The pH of both layers followed the same pattern throughout the experiment, in the SML pH was consistently ~0.9 units less than the ULW (**Fig. 2b**). Both layers had maximum pH values on day 19 at 8.73 and 8.67, respectively. Salinity showed a steady linear increase from day 1–31 for both layers, with near-identical measurements, ranging from 28.65 – 32.09 (**Fig. 2c**). The water temperature in the SML and ULW had a minimum of 17.03°C on day 9 and a maximum of 23.42°C in the SML on day 30, and 23.38°C on day 28 in the ULW (**Fig. 2d**).

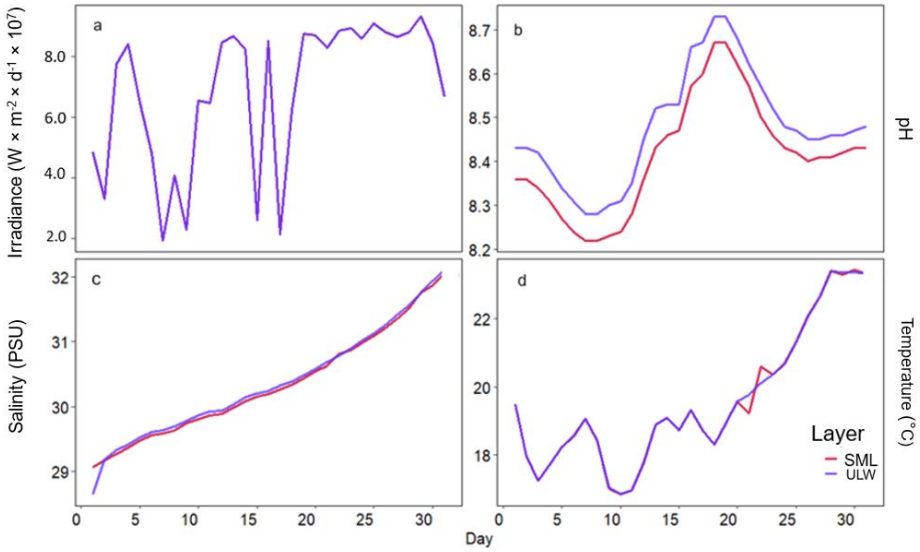


**Figure 2.** Physical environmental measurements taken throughout the experiment. Daily averages of irradiance W $m^{-2}$ $d^{-1}$ (a), pH (b), salinity PSU (c), and water temperatures °C (d). The daily averages of pH, salinity, and water temperature were calculated as minutely averages per day.

Chl *a* measurements showed a peak in concentration after each nutrient addition to 6.65 and 9.45 µg $L^{-1}$ (**Fig. 3a,** yellow triangles), followed by a decrease of 8.25 µg $L^{-1}$. Generally, DOC measurements in both the SML and ULW (**Fig. 3b**) started out low and increased over the course of the experiment. The minimum concentrations were 304.5 and 252.3 µM for the SML and ULW, respectively. DOC in the SML reached its maximum of 679 µM on day 29, whereas in the ULW DOC reached its highest concentration of 612 µM on day 22. Nitrate measurements in both layers started at maximum concentrations of 14.07 µM and 13.0 µM in the SML and ULW respectively (**Fig. 3c**). Both decreased to <1 µM on day 12 and remained low until day 32. Phosphate in the SML was very low until day 15 when it started to increase and reached its maximum concentration of 19.48 µM on day 28 (**Fig. 3d**). Phosphate in the ULW was generally around 0.19 µM, except on day 5 when a maximum concentration of 9.25 µM was measured. POC followed the same pattern as chlorophyll-a and ranged between 23.36–192.06 µM (**Fig.**

**3e**). Silicate concentrations were constant in both layers at ~1 µM until day 11 after which a sudden maximum of 17 µM was measured on day 12. Thereafter, the silicate concentrations decreased until the end of the experiment to 2.91 and 2.37 µM for the SML and ULW (**Fig. 3f**). DIC measurements were done with two different sampling methods, however those were not used across all dates and depths (data not shown). The minimum concentration was 1,695 µM in the SML, and the maximum was 2,204 µM. The maximum in the ULW was 2,150 µM and the minimum was 1,644 µM.

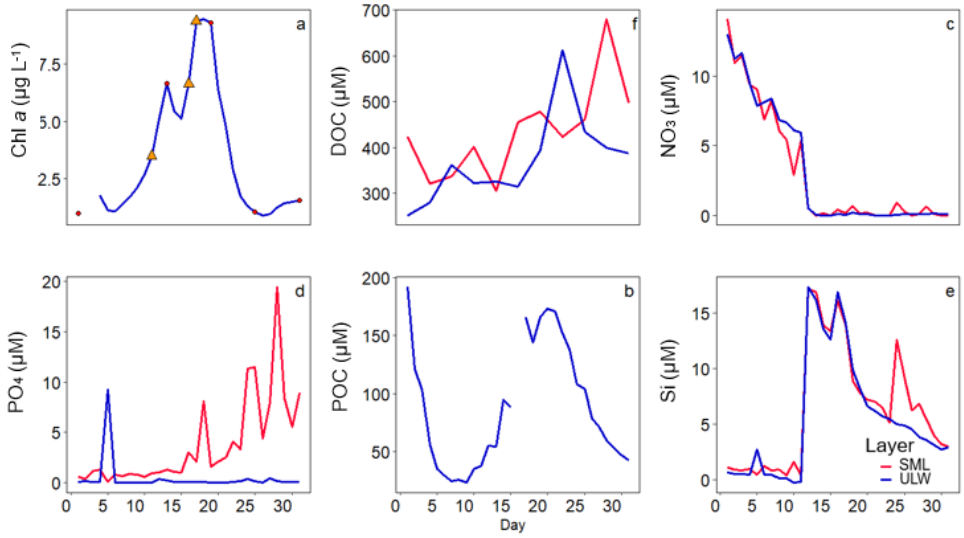


**Figure 3**. Chemical measurements during the experiment. Chl *a* concentrations (µg $L^{-1}$) (a), DOC in µM (b), $NO_3$ in µM (c), $PO_4$ in µM (d), POC in µM (e), and Si in µM (f). Yellow triangles in (a) indicate the nutrient additions. Red circles indicate the days of sample collection.

**Development of phytoplankton groups during the mesocosm experiment**

The abundance of algae in the mesocosm experiment was highest between days 18 to 21 (**Fig. 4**). The most abundant algae throughout the experiment were the Coccolithophyceae ranging from 0.39 –13 $\times 10^7$ cells $L^{-1}$. Flagellata made up the second most abundant algal group throughout the experiment, ranging from 0.28–3.70 $\times$ $10^7$ cells $L^{-1}$. Flagellata were present throughout the whole experiment with highest abundances occurring during and after the second Chl *a* maximum. Bacillariophyceae (diatoms) were the third most abundant class ranging from 0.003 – 2.2 $\times$ $10^7$ cells $L^{-1}$. With increasing algal abundances, the diversity of the diatom composition declined and vice versa, starting with 5 species (Bacillariales indet., Cylindrotheca Closterium, Pseudonitzschia seriata (complex), Thalassionema nitzschioides, and Rhizosolenia sp.) before the bloom, decreasing to 2 species (Cylindrotheca Closterium, Thalassiosira sp.) during the bloom, and increased again to 4 (Bacillariales indet., Cylindrotheca Closterium, Amphiprora sp., Rhizosolenia setigeraspecies) after the bloom. The Chlorophyta (cf.), Coscinodiscophyceae, Cryptophyceae, Dinophyceae, Mediophyceae, and

Prasinophyceae together made up only a few percent of the top 3 divisions ranging from absent to 545 cells $mL^{-1}$.

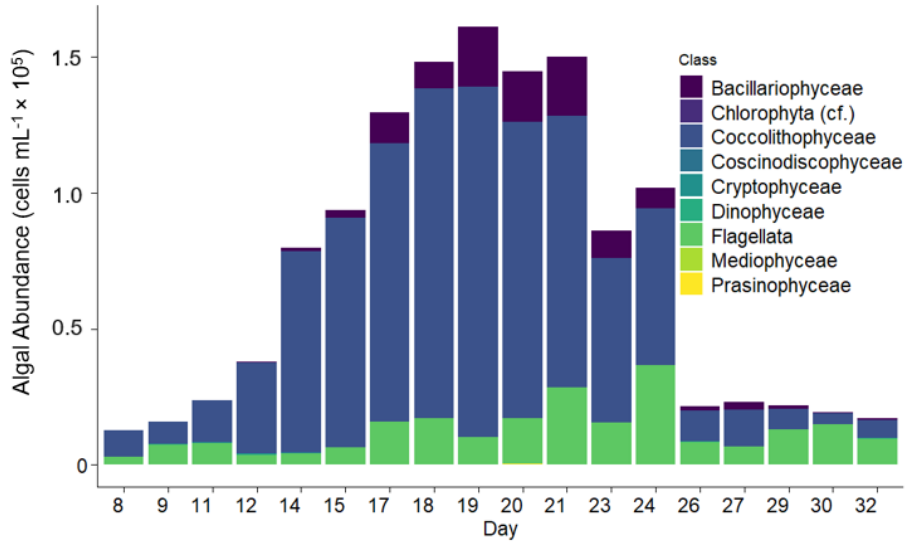


**Figure 4**. Species abundance data (cells $mL^{-1}$ x $10^5$) of phytoplankton during the mesocosm experiment grouped by class.

**Responses to the phytoplankton bloom of bacterial groups in the SML and ULW**

Crosstalk of cells between fluorescence channels can occasionally occur, thus testing for interference from the FISH channel into the DAPI channel is important to ensure accurate recovery of cells. The untreated filters mounted in DAPI mix directly showed abundances in the same range as the filters processed with the FISH protocol and no significant crosstalk between FISH and DAPI channel was detected (**Fig. 5**).

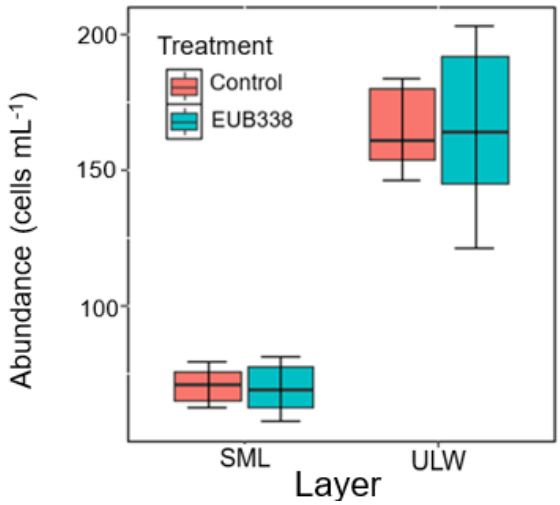


**Figure 5.** DAPI abundances in the SML and ULW on untreated filters compared to FISH filter sections with the EUB338 probe.

The absolute abundance of all bacteria fluorescing with the EUB338 probe in the SML (**Fig.6**) increased by ~ 9-fold from 0.98 × $10^6$ cells $mL^{-1}$ at the start of the experiment to 8.9 × $10^6$ cells $mL^{-1}$ during the peak of the Chl *a* bloom. In the ULW the minimum abundance of bacterial cells was counted on day 19 with 1.9 × $10^6$ cells $mL^{-1}$, while Chl *a* concentrations were highest. By day 31 there was a two-fold increase in bacterial cells.

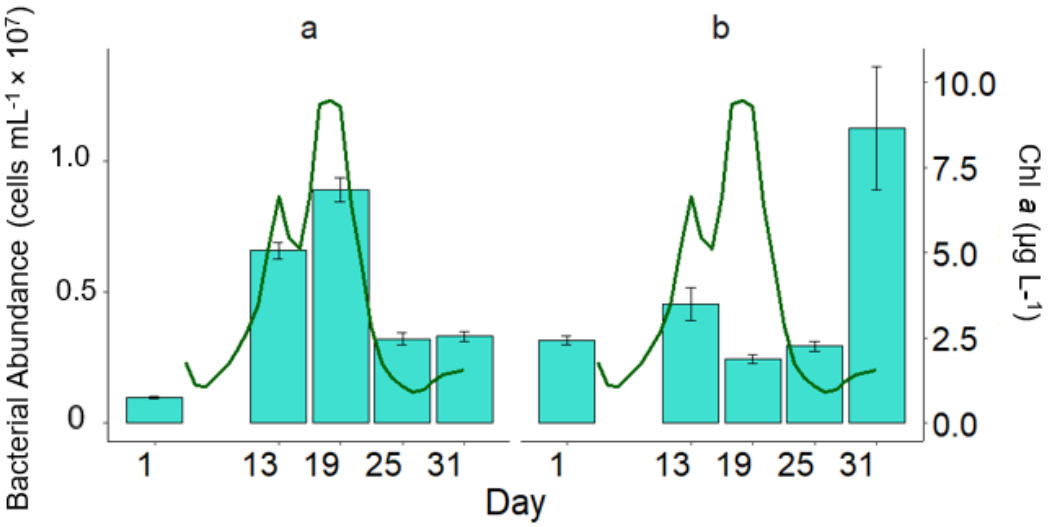


**Figure 6.** Absolute abundance of bacterial cells (cells $mL^{-1}$ x $10^7$) fluorescing with the EUB338 probe in the SML (a) and the ULW (b) compared to Chl *a* concentrations (green line) during the phytoplankton bloom.

The abundances of the three bacterial groups Bacteroidetes, Roseobacter, and SAR11 across both layers were roughly similar throughout the study, with SAR11 showing the lowest abundances overall (**Fig. 7a**). The lowest abundances of all three clades in the SML occurred on day 1, before the bloom, and the maximum on day 13, the first Chl *a* maximum. The abundance of Bacteroidetes increased by 2.6-fold from 0.68 to 1.8 × $10^6$ cells $mL^{-1}$ from day 1 to 13, Roseobacter by 3.7-fold from 0.57 to 2.1 × $10^6$ cells $mL^{-1}$, and SAR11 by ~22.7-fold from 0.11 to 2.5 × $10^6$ cells $mL^{-1}$. Overall, SAR11 showed the greatest increase in abundance, ~10x more than Bacteroidetes and Roseobacter, despite having the lowest abundances on every other sample day. In the ULW all three clades showed the lowest abundances on day 19 (**Fig. 7b**), corresponding with the peak of the bloom, after which bacterial abundance of all three groups increased substantially. Bacteroidetes had its maximum at the end of the experiment on day 31 while Roseobacter and SAR11 both experienced highest abundances directly after the bloom on day 25. Bacteroidetes increased ~ 10-fold from 0.27 to 2.7 × $10^6$ cells $mL^{-1}$. Roseobacter increased by 4.7-fold from 0.47 to 2.2 × $10^6$ cells $mL^{-1}$, and SAR11 by 6.2-fold from 0.29 to 1.8 × $10^6$ cells $mL^{-1}$. The maximum abundance of Bacteroidetes in the ULW was

1.5x greater than the maximum in the SML, the maximum of Roseobacter in the ULW was roughly the same as the maximum in the SML, and in contrast, the maximum of SAR11 was 1.4x greater in the SML compared to the ULW.

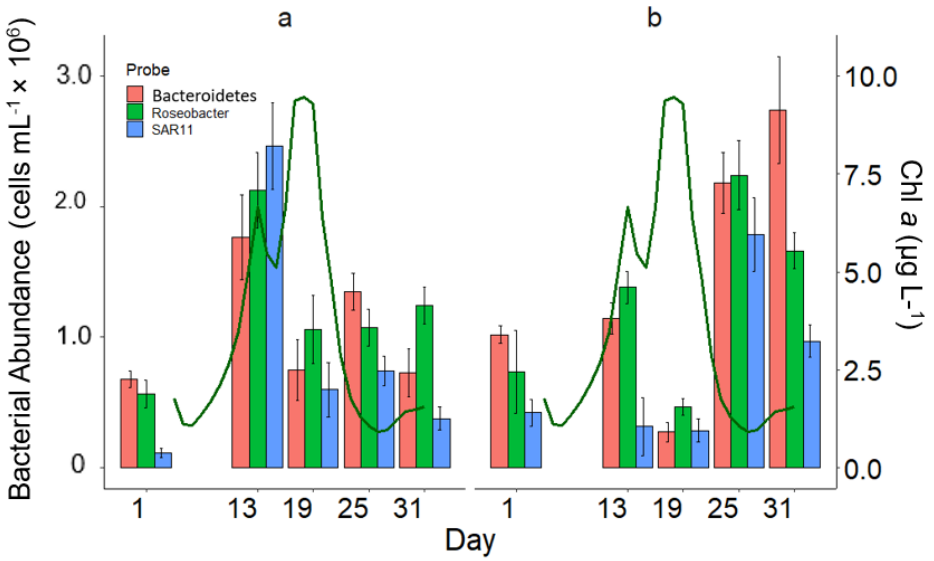


**Figure 7.** Absolute abundance of FISH-positive cells for the bacterial groups Bacteroidetes, Roseobacter, and SAR11 in the SML (a) and ULW (b) against Chl *a* measurements (green line).

**Dynamics of active bacteria during the phytoplankton bloom**

The abundance of all active bacterial cells (Click-positive cells from EUB338) followed the same pattern as the abundances from the three specific bacterial groups in the SML and ULW (**Fig. 7**) but differed from the abundances from the general bacteria (FISH-positive cells from EUB338; **Fig. 6**). The abundance of active bacteria in the SML increased by 14-fold from 0.27 to 3.8 × $10^6$ cells $mL^{-1}$, between days 1 and 13 (**Fig. 8**). On day 13 the peak abundance of active bacterial cells made up 58% of all bacterial cells present in the SML. In the ULW the maximum abundance occurred on day 31, with active cells making up 29% of all bacteria, however, the greatest proportion of active cells occurred directly after the bloom on day 25, at 59% of cells being active.

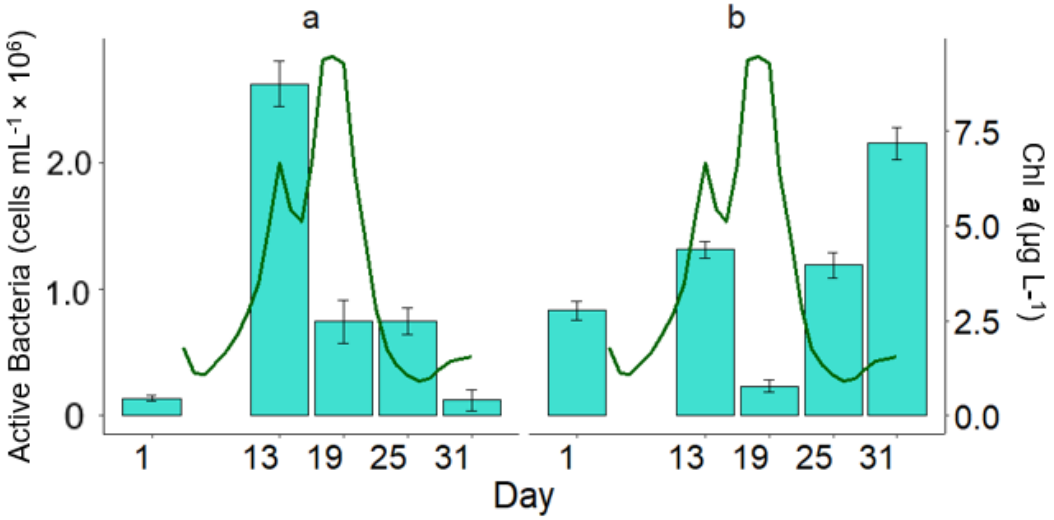


**Figure 8.** Abundance of all active bacterial cells fluorescing with the EUB338 probe in the SML (a) and ULW (b) against chlorophyll-a concentrations (green line).

The abundance of active Bacteroidetes cells followed a very similar pattern to the absolute FISH abundances in the SML (**Fig. 9, a**). The abundance ranged from 0.07 to 0.79 × $10^6$ cells $mL^{-1}$, an 11-fold increase, its minimum on day 1 and maximum on day 13. The active abundance of Roseobacter followed the same distribution pattern as Bacteroidetes but with a range of 0.1 to 1.4 × $10^6$ cells $mL^{-1}$, increasing by 14-fold in the same time. SAR11 in the SML also followed this pattern with a range of 0.017 to 1.06 × $10^6$ cells $mL^{-1}$, showing a 62.4-fold increase. The absolute abundance of active Bacteroidetes cells in the ULW (**Fig. 9, b**) followed the same distribution patterns of both the absolute FISH (**Fig. 7, b**) and all active bacterial cells (**Fig.8**), ranging from 0.07 to 2.0 × $10^6$ cells $mL^{-1}$, a 28.6-fold increase. Roseobacter and SAR11 both followed similar distributions with ranges of 0.17 to 1.6 × $10^6$ and 0.37 to 8.9 × $10^5$ cells $mL^{-1}$ respectively. These abundances were 9.4-fold and 24-fold increases of Roseobacter and SAR11.

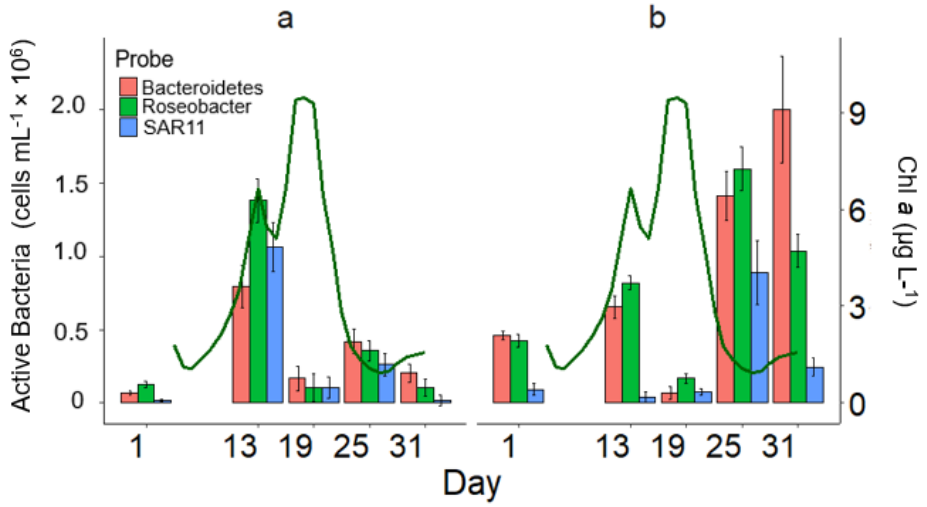


**Figure 9**. Abundance of active cells per bacterial group in the SML (a) and ULW (b) against Chl *a* concentrations (green line).

The Wilcoxon signed-rank test was used to determine significant differences between bacterial abundances of the SML and ULW throughout the experiment. The test was performed on the total abundance as determined by the single FISH probes in the SML against the total abundance of combined groups from the ULW. To obtain a more detailed insight into the bacterial abundances during the bloom, abundances from the SML and ULW were assigned to one of three phases of the bloom according to their sample day and its corresponding Chl *a* concentration. Phase 1 included all abundances from day 1 to 12 and was considered the pre-bloom phase. Phase 2 included abundances from days 13 and 19, when the bloom was at its peak and phase 3 included all abundances from days 25 and 31 with declining Chl *a* concentrations and was considered the post-bloom phase. The Wilcoxon test was performed between the SML and ULW for each phase of the bloom. The same was done with the active bacterial abundances from the Click analyses (**see Table 2)**.

The first phase of the bloom showed no significant difference between the bacterial abundances of the SML and ULW for either the total abundances or the active abundances. Phase two of the bloom, when Chl *a* concentrations were high, showed a significant difference in the total bacterial abundance between the SML and ULW, for both the total and active abundances with *p*-values of 0.002 and 0.023 respectively. During phase three both the total and active bacterial abundances were significantly different between the layers, the total abundances showed a *p*-value of 0.004 and the active abundances a *p*-value of 0.008. In phase two of both the total and active abundances the SML clearly has significantly higher abundances than the ULW (**Fig. 7** and **8**). In phase 3 it is the opposite, the ULW has significantly higher abundances than the SML for both abundance and activity.

**Table 2.** P values of Wilcoxon signed rank tests on abundances of FISH and Click analyses in the SML and ULW. The tests were performed using all probes including EUB338 and ALF968.

| Bloom Phase | Total[a] *p*-value | Active[b] *p*-value |
|---|---|---|
| 1 | 0.0625 | 0.125 |
| 2 | 0.002* | 0.023* |
| 3 | 0.004* | 0.008* |
| **All phases** | **0.751** | **0.143** |

[a]denotes Wilcoxon *p*-values based on combined abundances of FISH probes.
[b]denotes Wilcoxon *p*-values based on combined abundances from Click-It analyses.
**p*-values < 0.05

**Dynamics of bacterial groups during the development of the phytoplankton bloom**

Microbial growth was modelled using the growthcurver function in R based on abundance counts of the single samples. For each bacterial group and analysis type (DAPI, FISH, Click) from both the SML and ULW the potential initial population size (*n0*), carrying capacity (*k*), and growth rate (*r*) were calculated (**Table 3**). Fitting the abundance data from each bacterial group and layer to the logistic growth curve implemented in the model revealed that the DAPI and FISH abundances (using the EUB338 probe mix) in the SML closely followed the logistic growth curve (**Fig. S1, supplementary info**). The DAPI abundances indicated a growth rate of 6% per hour and a carrying capacity of $6.0 \times 10^6$ cells, exceeding the carrying capacity by day 13 with a population of $9.6 \times 10^6$ cells. The growth leveled off and remained stable throughout the remainder of the study. The FISH abundances in the SML followed the same growth pattern, with a 7% increase per hour, exceeding it carrying capacity by 62%. The active abundances from the SML did not fit the logistic growth equation and could not be fitted to the model. All bacteria (EUB338) from the ULW appears to more closely follow an exponential growth curve as the population increases rapidly towards the end of the experiment. This led to a significantly lower overall growth rate than that of the SML, at 0.3% per hour. Despite increasing exponentially in the final days of the experiment, the bacterial carrying capacity of $9.8 \times 10^{13}$ cells was not close to being reached as the final recorded population size was $1.1 \times 10^7$ cells. Click abundances in the ULW from all bacteria, Bacteroidetes, Roseobacter, and SAR11 were able to be fitted to the logistic growth curve, and given the shape of the curves, the active bacterial abundances from all bacteria and Bacteroidetes in the ULW were just approaching the rapid growth phase and Roseobacter and SAR11 were still in the slow growth phase.

**Table 3.** Growthcurver summary statistics generated from each bacterial group, fluorescent cell type (DAPI, FISH, or Click) and layer (SML and ULW). Statistics are related to the logistic growth curve formula, showing carrying capacity (*k*), initial population size (*n0*), and growth rate (*r*).

| ***Bacterial Group*** | ***Cell type*** | ***Layer*** | ***k*** | ***n0*** | ***r*** |
|---|---|---|---|---|---|
| EUB338 | DAPI | SML | $6.0 \times 10^6$ | 437454 | 0.064 |
| Bacteroidetes | DAPI | ULW | $1.0 \times 10^{13}$ | 3079645 | 0.001 |
| SAR11 | DAPI | SML | $7.0 \times 10^6$ | 567367 | 0.067 |
| SAR11 | DAPI | ULW | $4.2 \times 10^6$ | 1526741 | 0.062 |
| EUB338 | FISH | SML | $5.5 \times 10^6$ | 213695 | 0.070 |
| EUB338 | FISH | ULW | $9.4 \times 10^{13}$ | 675355 | 0.004 |
| Bacteroidetes | FISH | ULW | $1.0 \times 10^{13}$ | 397825 | 0.003 |
| SAR11 | FISH | ULW | $1.4 \times 10^6$ | 0 | 0.060 |
| EUB338 | Click | ULW | $9.5 \times 10^{12}$ | 455364 | 0.002 |
| Bacteroidetes | Click | ULW | $7.4 \times 10^{12}$ | 118666 | 0.004 |
| Roseobacter | Click | ULW | $2.7 \times 10^6$ | 360097 | 0.002 |
| SAR11 | Click | ULW | $5.6 \times 10^5$ | 0 | 0.051 |

## Correlations of environmental variables and bacterial abundances

To identify the environmental parameters influencing microbial abundances during the mesocosm experiment, Spearman's rank correlation tests were performed on total bacterial abundance and activity in both layers. In the SML (**Fig. 10a**) the abundance of DAPI cells showed a positive correlation with the Chl *a* data (measurements from the ULW) and negative correlations with salinity and phosphate. FISH abundances correlated positively with silicate and negatively with DOC, phosphate, pH, and nitrate. The absolute abundances of active cells negatively correlated with DOC, salinity, and Chl *a*. The hclust similar variables hierarchically, the most apparent being FISH, Click, and silicate negatively correlated with DOC. Spearman correlations in the ULW (**Fig. 10b**) indicated a postive correlation of DAPI abundances with phosphate as opposed to Chl *a* in the SML. FISH abundances were positively correlated and clustered with temperature and nitrate. In a separate cluster FISH was strongly negatively associated with Chl *a*, moderately with POC, and weakly but positivly with DOC. The active abundance correlations were in the same cluster, negatively associated with silicate and pH.

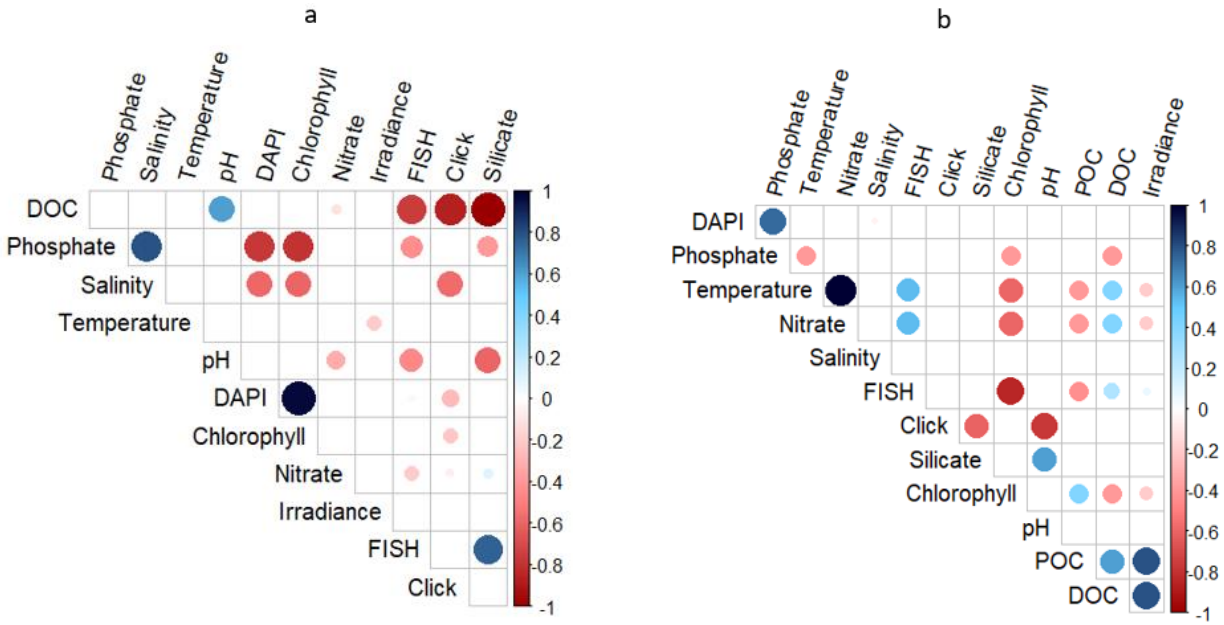


**Figure 10.** Spearman rank correlation matrix of abundances and environmental parameters in the SML (a) and the ULW (b). Blue circles indicate positive correlations while red circles indicate negative correlations. Darker and larger circles correspond to the strength of the correlation, lighter and smaller circles indicating weak correlations.

## *Discussion*

The aim of this study was to address the dynamics of bacterial assemblages in the SML and the ULW during an induced phytoplankton bloom in a mesocosm. While earlier studies of bacteria in the SML have investigated bacterial diversity and the differences between the layers, this study explicitly focused on which environmental parameters drive the observed bacterial differences and dynamics. In our study the bacterial abundances and activity were statistically distinct between the SML and ULW during the second and third phase of the algal bloom (**Table 2**). The main drivers for this distinction were found to be concentrations of DOC, Chl *a*, and POC, with DOC negatively correlating with the abundance and activity in the SML while positively correlating with the abundances in the ULW (**Fig. 11** and **12**). The bacterial abundance and activity followed the succession of the dominating algae predominately in the ULW during the third phase of the bloom (**Fig. 7b** and **9b**) in which the algae shifted from being dominated by Coccolithophyceae to Flagellata, and the dominating bacterial group shifted from Roseobacter to Bacteroidetes on day 31 of the experiment (**Fig. 4**).

### Artificial bloom microbial dynamics vs. natural phytoplankton blooms of the North Sea

The dynamics of bacterial abundance in this experiment is similar to another mesocosm study following bacterial abundances and production. Riemann et al. (2000) used different methodologies to obtain bacterial abundance and production and also investigated only one

depth layer, but the bacterial abundances also showed an increase with increasing Chl *a* concentrations in Alphaprotebacteria (Roseobacter and SAR11) and Cytophagales (Bacteroidetes) and both groups decreased dramatically after the peak of the phytoplankton bloom. While both experiments saw an increase in bacterial activity after the Chl *a* maximum, ULW abundances in our experiment (**Fig. 7b**) reached their peak at this time, whereas the SML of our experiment (**Fig. 7a**) and the Riemann abundances peaked right before the Chl *a* peak. The active bacterial abundance of both the ULW from our experiment (**Fig. 9b**) and the Riemann experiment peaked after the Chl *a* peak, while the active abundance in the SML from our study (**Fig. 9a**) peaked at the beginning of the bloom (Riemann et al. 2000).

Similar to the results of our study, Wemheuer et al. (2015) found high numbers of Alphaproteobacteria (~50%) and Bacteroidetes (~20%) in a North Sea spring phytoplankton bloom. However, a lower abundance of SAR11 in the bloom as compared to a sampled patch outside the bloom was found which contradicted our findings. In our mesocosm the SAR11 abundances in the SML were the highest of all bacterial groups during the beginning of the induced bloom (**Fig. 7a**). Yet another study found SAR11 abundances highest during the pre-bloom and bloom phases (Sidhu et al. 2023). In the ULW, SAR11 from our study was lowest in abundance during the peak of the bloom, aligning with the findings of Wemheuer et al. (2015), and increased substantially after the bloom. The low SAR11 abundances in the presence of the bloom in the Wemheuer study could be due to the bloom phase in which the samples were collected, as well as the depth (neither were stated in the methodology of the Wemheuer study). Thus, it appears that the dynamics of SAR11 in the SML of our mesocosm closely resemble the results of Sidhu et al. (2023), while the changes in the ULW closely align with Wemheuer et al. (2015), indicating distinct members of the SAR11 clade are present within the two layers. A major difference between the findings from Wemheuer et al. (2015) and our mesocosm is the presence of Gammaproteobacteria. In the natural samples from Wemheuer, Gammaproteobacteria make up a similar portion of the community composition as Bacteroidetes, and an even larger portion of the active community composition, whereas the Gammaproteobacteria in our experiment were too low in abundance to conduct sensible FISH or Click analysis. The active abundance of Bacteroidetes in the presence of the bloom from the Wemheuer study was slightly higher than in the total community and higher than the activity of the non-bloom samples. The SAR11 abundance in the active community was almost non-existent within the bloom samples, only slightly more-so in the non-bloom samples, despite contributing to a sizable portion of the total community in both the bloom and non-bloom samples. In contrast, our study showed Bacteroidetes as the most active bacterial group

throughout the experiment, peaking at the end of the bloom when Chl *a* concentrations were low (**Fig. 9**). The Alphaproteobacteria in our study (SAR11 and Roseobacter) seem to contribute a similar amount to the active community as in the Wemheuer study however, SAR11 in our study is more significant, especially in the SML bloom phase.

**Impact of environmental parameters on bacterial groups**

To gain a more detailed insight into the correlations between the abundance and activity of specific bacterial groups and environmental parameters a redundancy analysis (RDA) of the abundances of FISH-positive and Click-positive cells was performed. We used three environmental variables that generally influence the bacterial abundances in the ocean and chose DOC, nitrate, and temperature to be the most informative. In the RDA these three variables together make up 87% of the constrained variance, with 12.5% unconstrained variance, meaning these three factors account for the majority of variation we see in the bacterial abundance and activity while they cannot explain a relatively small amount of that variation. Bacteroidetes and Roseobacter abundance and activity were positively correlated with temperature and nitrate, while total bacterial abundance and activity were negatively correlated (**Fig. 11).** DOC had the strongest influence on the abundance and activity of SAR11, while nitrate and temperature drove the overall variance in the response variable (69.4% of the constrained variance explained by RDA axis 1). The negative correlation of DOC with the total and active SAR11 abundances suggest that higher concentrations of DOC resulted in lower abundance and activity of SAR11. Because RDA axis 2 accounts for a smaller portion of the constrained variance (18.05%), finer distinctions in the relationships between the abundance data and environmental variables are observed as SAR11 abundance and activity are the highest response variables along the vertical axis, and negatively associated with DOC. The positioning of the remaining bacterial groups near 0 on the RDA2 axis reveals an overall weak correlation with RDA2 but given that they all reside on the lower portion of the graph along the with environmental arrows shows that the correlation is positive, mainly to DOC.

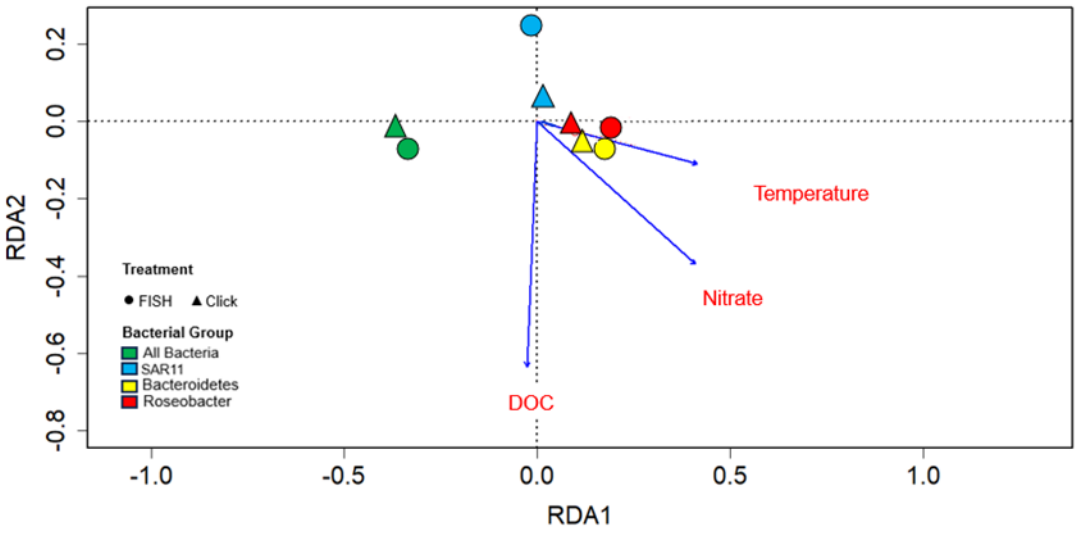


**Figure 11.** Redundancy analysis using z-scores from selected environmental variables and Hellinger-transformed absolute FISH and Click abundances of Bacteroidetes, Roseobacter, SAR11, and Bacteria from the SML.

Similar to the SML, a redundancy analysis was conducted for the ULW with Chl *a*, DOC, and POC as the parameters of choice. These variables contributed 61.6% of the total variance in the response data (**Fig. 12**). With 75.4% of the constrained variance (46.4% of total variance) explained by RDA axis 1, the response variables are separated along the gradient of Chl *a* and DOC. Chl *a* is positively correlated with total bacterial (EUB338) abundance and activity and negatively correlated with the abundance and activity of Bacteroidetes. DOC on the other hand strongly correlated with the abundance of SAR11, which is in contrast to SAR11 in the SML correlating negatively with DOC. Thus, these trends in DOC requirements of SAR11 suggest the presence of distinct subgroups of SAR11 in the two layers, which is also indicated by the dynamics in the abundances along the development of the bloom. RDA axis 2 explains 21.4% of the constrained variance (13.2% total variance) of the response variables and is primarily driven by POC. Bacteroidetes abundance and activity are both negatively correlated with POC and Roseobacter abundance and activity show a weaker but positive correlation to POC (**Fig. 12)**.

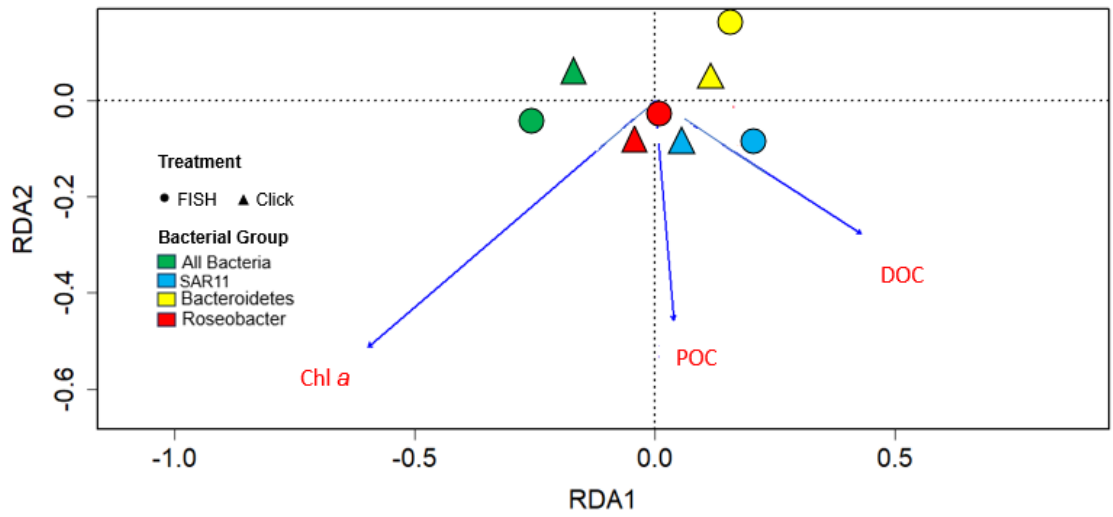


**Figure 12.** RDA using the absolute FISH and Click abundances from the ULW using the Hellinger transformation. Environmental variables have been transformed with z-scoring.

The information provided from fitting the abundance data to the logistic growth curve further reveals which environmental factors drive the growth of the specific bacterial groups' abundance and activity. The total abundance (EUB338) in the SML reached its carrying capacity by day 13 (**Fig. S1**), right as the nitrate concentrations were depleted, suggesting that nitrate is the limiting nutrient for the majority of bacteria in the SML. The total abundance (EUB338) in the ULW began increasing exponentially around day 19 of the experiment, the same time that temperature measurements steadily began increasing. As was revealed in the redundancy analysis, a negative correlation of total bacterial activity with DOC was present, and when looking at the fitted growth curve it appears that the DOC was taken up rapidly starting on day 23, decreasing to pre-bloom levels by the end of the study. During this time, the bacterial growth increased exponentially, thus revealing DOC as a driving force for the growth rate of bacteria in the ULW.

**Potential Issues in Methodology**

We originally intended to count actively respiring bacterial cells, however, we discovered during trial runs that the signals emitted in this channel were of extremely poor quality. We hypothesize that the incubation with formaldehyde to fix microbial cells is not compatible with the Redox Sensor Green fluorophore and further testing of fixatives is needed.

In the FISH analyses the ALF968 probe was used to target all Alphaproteobacteria while the probes SAR11-441R and Roseo563R were employed to study the subgroups Pelagibacteraceae SAR11 and Roseobacter, respectively. Given that ALF968 should target all cells that are part

of Alphaproteobacteria, its relative abundance should always be greater than or equal to the combined abundances of the subgroups. However, this was not the case for all samples and particularly on day 25 in the ULW, cell counts using ALF968 indicated a nearly 50% lower abundance compared to the other two probes combined (**Fig. 13**). For all probes we worked with the suggested formamide concentrations and hybridization conditions, however, we assume that occasionally the competitor probe RoseoC563R does not work properly due to the sample matrix and may skew the Roseobacter abundances. Another possible explanation is that not enough competitor probe was added to the sample and further testing to determine the correct amount is required.

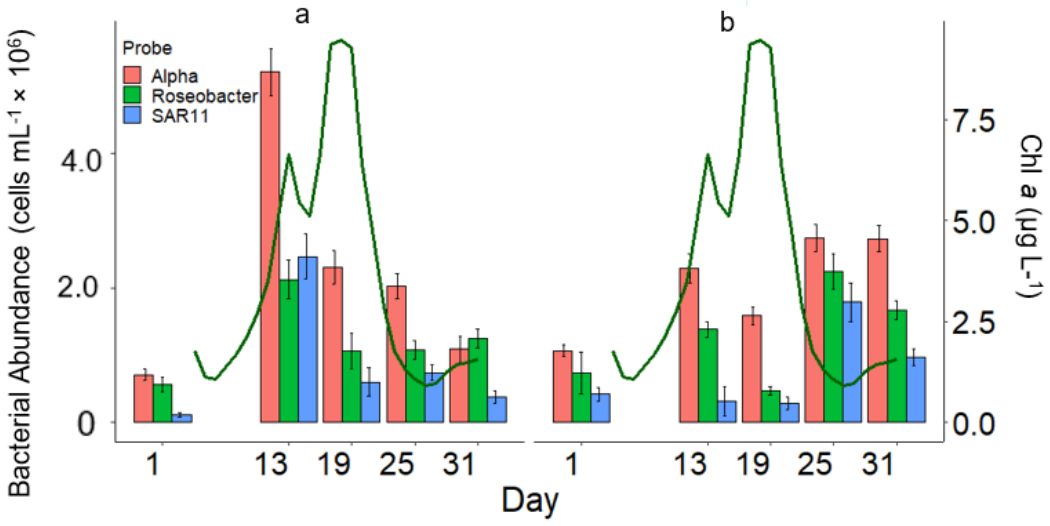


**Figure 13.** Abundances of Alphaproteobacteria hybridized to the FISH probe ALF968 and abundances of the subgroups Roseobacter and SAR11 in the SML (a) and ULW (b). Error bars show standard error, and the green line represents Chl a concentrations in the mesocosm.

## Conclusions

The microbial communities in the SML and the ULW show distinct differences in both abundance and activity of the bacteria as well as the biotic and abiotic parameters driving these differences. While there was lower overall activity in the SML as compared to the ULW, the SML saw increased abundances and activity during the active bloom phase , while the ULW saw higher increases post-bloom. Variability in the organic matter due to changes in algal composition and its decomposition in the course of the experiment played a key role because the dominant bacterial groups seemed to follow the changes in succession of the substrate. This is evident in the SML as the starting phase of the bloom was dominated by SAR11, coinciding with a sharp increase of Coccolithophyceae. The dominance of the Roseobacter group was followed by Bacteroidetes and changed back again to Roseobacter. This back and forth was paralleled by an increase in silicate concentration and abundance of flagellata. We found

extremely low abundances and activity of SAR11 in the ULW at the start of the bloom which was in stark contrast to the SML. We suggest that different members of the SAR11 clade are inhabiting the SML and ULW, as the SAR11 in the ULW does not appear to be adapted to utilizing the fresh organic matter from the Coccolithophyceae. Rather, it reaches a maximum abundance in the post-bloom phase where it might benefit from the older DOC of slightly different molecular composition. Also, Bacteroidetes and Roseobacter in ULW show higher abundances and activity in the post-bloom phase. This might be either due to a preference for the post-bloom substrate composition, or due to delayed accessibility of the DOM from sinking of particulate organic matter into the ULW.

The effects of UVA and UVB radiation on bacterial activity in the SML could not be determined, as only daily integrat1ed solar radiation across all wavelengths was available. No direct correlations between bacterial abundance or activity and daily irradiance were observed in either the SML or ULW. Since the experiment, conducted in the spring, was not subject to high UV radiation levels, its impact on bacterial DNA damage and subsequent activity in the SML was likely minor. However, to conclusively rule out UV radiation as a driving factor, further studies differentiating radiation types are needed. Such studies could clarify whether UVA or UVB radiation differentially affects the labile versus refractory fractions of DOM, potentially altering DOM composition and influencing which bacterial groups can benefit.

## Supplementary Information

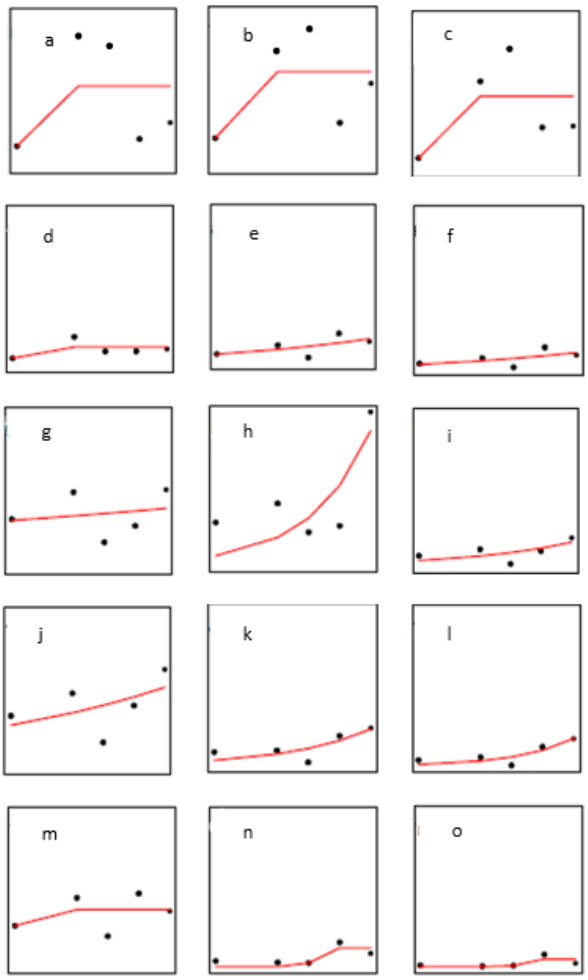


**Figure S1.** Logistic growth curves for all samples fitting the model as abundances over time. DAPI cells from the EUB338 probe in the SML (a), EUB338 FISH cells in the SML (b), DAPI cells from the SAR11 sample in the SML (c), Roseobacter cells in the SML (d), Roseobacter cells in the ULW (e), active Roseobacter cells in the ULW (f), DAPI cells from EUB338 sample in the ULW (g), all bacterial cells in the ULW (h), all active bacterial cells in the ULW (i), DAPI cells from the Bacteroidetes sample in the ULW (j), Bacteroidetes cells in the ULW (k), active Bacteroidetes cells in the ULW (l), DAPI cells from the SAR11 samples in the ULW (m), SAR11 cells in the ULW (n), active SAR11 cells in the ULW.

## References


Agogué, H., E. O. Casamayor, M. Bourrain, I. Obernosterer, F. Joux, G. J. Herndl, and P. Lebaron. 2005. A survey on bacteria inhabiting the sea surface microlayer of coastal ecosystems. FEMS Microbiology Ecology **54**: 269–280. doi:10.1016/j.femsec.2005.04.002

Alderkamp, A., E. Sintes, and G. Herndl. 2006. Abundance and activity of major groups of prokaryotic plankton in the coastal North Sea during spring and summer. Aquat. Microb. Ecol. **45**: 237–246. doi:10.3354/ame045237

Amann, R. I., W. Ludwig, and K. H. Schleifer. 1995. Phylogenetic identification and in situ detection of individual microbial cells without cultivation. Microbiological Reviews **59**: 143–169. doi:10.1128/mr.59.1.143-169.1995

Arnds, J., K. Knittel, U. Buck, M. Winkel, and R. Amann. 2010. Development of a 16S rRNA-targeted probe set for Verrucomicrobia and its application for fluorescence in situ hybridization in a humic lake. Systematic and Applied Microbiology **33**: 139–148. doi:10.1016/j.syapm.2009.12.005

Bakenhus, I., L. Dlugosch, S. Billerbeck, H.-A. Giebel, F. Milke, and M. Simon. 2017. Composition of Total and Cell-Proliferating Bacterioplankton Community in Early Summer in the North Sea – Roseobacters Are the Most Active Component. Frontiers in Microbiology **8**.

Bennke, C. M., G. Reintjes, M. Schattenhofer, A. Ellrott, J. Wulf, M. Zeder, and B. M. Fuchs. 2016. Modification of a High-Throughput Automatic Microbial Cell Enumeration System for Shipboard Analyses. Applied and Environmental Microbiology **82**: 3289–3296. doi:10.1128/AEM.03931-15

Brüwer, J. D. and others. 2023. In situ cell division and mortality rates of SAR11, SAR86, Bacteroidetes, and Aurantivirga during phytoplankton blooms reveal differences in population controls. mSystems **8**: e01287-22. doi:10.1128/msystems.01287-22

Calleja, M. Ll., C. M. Duarte, N. Navarro, and S. Agustí. 2005. Control of air-sea CO2 disequilibria in the subtropical NE Atlantic by planktonic metabolism under the ocean skin. Geophysical Research Letters **32**. doi:10.1029/2004GL022120

Daims, H., A. Brühl, R. Amann, K.-H. Schleifer, and M. Wagner. 1999. The Domain-specific Probe EUB338 is Insufficient for the Detection of all Bacteria: Development and Evaluation of a more Comprehensive Probe Set. Systematic and Applied Microbiology **22**: 434–444. doi:10.1016/S0723-2020(99)80053-8

Dickson, A. G., C. L. Sabine, and J. R. Christian. 2007. Guide to Best Practices for Ocean CO2 Measurements. Report North Pacific Marine Science Organization.

Doane, T. A., and W. R. and Horwáth. 2003. Spectrophotometric Determination of Nitrate with a Single Reagent. Analytical Letters **36**: 2713–2722. doi:10.1081/AL-120024647

Eilers, H., J. Pernthaler, F. O. Glöckner, and R. Amann. 2000. Culturability and In Situ Abundance of Pelagic Bacteria from the North Sea. Appl Environ Microbiol **66**: 3044–3051. doi:10.1128/AEM.66.7.3044-3051.2000

Franklin, M. P., I. R. McDonald, D. G. Bourne, N. J. P. Owens, R. C. Upstill-Goddard, and J. C. Murrell. 2005. Bacterial diversity in the bacterioneuston (sea surface microlayer): the bacterioneuston through the looking glass. Environmental Microbiology **7**: 723–736. doi:10.1111/j.1462-2920.2004.00736.x

del Giorgio, P. A., and J. J. Cole. 1998. Bacterial Growth Efficiency in Natural Aquatic Systems. Annual Review of Ecology and Systematics **29**: 503–541. doi:10.1146/annurev.ecolsys.29.1.503

Harvey, G. W., and L. A. Burzell. 1972. A Simple Microlayer Method for Small Samples. Limnology and Oceanography **17**: 156–157. doi:10.4319/lo.1972.17.1.0156

Herndl, G. J., G. Müller-Niklas, and J. Frick. 1993. Major role of ultraviolet-B in controlling bacterioplankton growth in the surface layer of the ocean. Nature **361**: 717–719. doi:10.1038/361717a0

Ipcc. 2022. Global Warming of 1.5°C: IPCC Special Report on Impacts of Global Warming of 1.5°C above Pre-industrial Levels in Context of Strengthening Response to Climate Change, Sustainable Development, and Efforts to Eradicate Poverty, 1st ed. Cambridge University Press.

Lancelot, C., and G. Billen. 1984. Activity of heterotrophic bacteria and its coupling to primary production during the spring phytoplankton bloom in the southern bight of the North Sea. Limnology and Oceanography **29**: 721–730. doi:10.4319/lo.1984.29.4.0721

Leizeaga, A., M. Estrany, I. Forn, and M. Sebastián. 2017. Using Click-Chemistry for Visualizing in Situ Changes of Translational Activity in Planktonic Marine Bacteria. Frontiers in Microbiology **8**.

Manz, W., R. Amann, W. Ludwig, M. Wagner, and K.-H. Schleifer. 1992. Phylogenetic Oligodeoxynucleotide Probes for the Major Subclasses of Proteobacteria: Problems and Solutions. Systematic and Applied Microbiology **15**: 593–600. doi:10.1016/S0723-2020(11)80121-9

Manz, W., G. Arp, G. Schumann-Kindel, U. Szewzyk, and J. Reitner. 2000. Widefield deconvolution epifluorescence microscopy combined with fluorescence in situ hybridization reveals the spatial arrangement of bacteria in sponge tissue. J Microbiol Methods **40**: 125–134. doi:10.1016/s0167-7012(99)00103-7

Morris, R. M., M. S. Rappé, S. A. Connon, K. L. Vergin, W. A. Siebold, C. A. Carlson, and S. J. Giovannoni. 2002. SAR11 clade dominates ocean surface bacterioplankton communities. Nature **420**: 806–810. doi:10.1038/nature01240

Munson-McGee, J. H. and others. 2022. Decoupling of respiration rates and abundance in marine prokaryoplankton. Nature **612**: 764–770. doi:10.1038/s41586-022-05505-3

Murchie, E. H., and T. Lawson. 2013. Chlorophyll fluorescence analysis: a guide to good practice and understanding some new applications. Journal of Experimental Botany **64**: 3983–3998. doi:10.1093/jxb/ert208

Obernosterer, I. and others. 2008. Biochemical characteristics and bacterial community structure of the sea surface microlayer in the South Pacific Ocean. Biogeosciences **5**: 693–705. doi:10.5194/bg-5-693-2008

Obernosterer, I., P. Catala, T. Reinthaler, G. Herndl, and P. Lebaron. 2005. Enhanced heterotrophic activity in the surface microlayer of the Mediterranean Sea. Aquat. Microb. Ecol. **39**: 293–302. doi:10.3354/ame039293

Reinthaler, T., E. Sintes, and G. J. Herndl. 2008. Dissolved organic matter and bacterial production and respiration in the sea-surface microlayer of the open Atlantic and the western Mediterranean Sea. Limnology and Oceanography **53**: 122–136. doi:10.4319/lo.2008.53.1.0122

Reintjes, G., B. M. Fuchs, M. Scharfe, K. H. Wiltshire, R. Amann, and C. Arnosti. 2020. Short-term changes in polysaccharide utilization mechanisms of marine bacterioplankton during a spring phytoplankton bloom. Environmental Microbiology **22**: 1884–1900. doi:10.1111/1462-2920.14971

Riemann, L., G. F. Steward, and F. Azam. 2000. Dynamics of Bacterial Community Composition and Activity during a Mesocosm Diatom Bloom. Applied and Environmental Microbiology **66**: 578–587. doi:10.1128/AEM.66.2.578-587.2000

Rink, B., S. Seeberger, T. Martens, D. Duerselen C, M. Simon, and T. Brinkhoff. 2007. Effects of phytoplankton bloom in a coastal ecosystem on the composition of bacterial communities. Aquat. Microb. Ecol. **48**: 47–60. doi:10.3354/ame048047

Roesler, C. S., and A. H. Barnard. 2013. Optical proxy for phytoplankton biomass in the absence of photophysiology: Rethinking the absorption line height. Methods in Oceanography **7**: 79–94. doi:10.1016/j.mio.2013.12.003

Samset, B. H., J. S. Fuglestvedt, and M. T. Lund. 2020. Delayed emergence of a global temperature response after emission mitigation. Nat Commun **11**: 3261. doi:10.1038/s41467-020-17001-1

Sharp, J. H. 1974. Improved analysis for “particulate” organic carbon and nitrogen from seawater. Limnology and Oceanography **19**: 984–989. doi:10.4319/lo.1974.19.6.0984

Sidhu, C. and others. 2023. Dissolved storage glycans shaped the community composition of abundant bacterioplankton clades during a North Sea spring phytoplankton bloom. Microbiome **11**: 77. doi:10.1186/s40168-023-01517-x

Tolli, J. D., S. M. Sievert, and C. D. Taylor. 2006. Unexpected Diversity of Bacteria Capable of Carbon Monoxide Oxidation in a Coastal Marine Environment, and Contribution of the Roseobacter-Associated Clade to Total CO Oxidation. Appl Environ Microbiol **72**: 1966–1973. doi:10.1128/AEM.72.3.1966-1973.2006

Wallner, G., R. Amann, and W. Beisker. 1993. Optimizing fluorescent in situ hybridization with rRNA-targeted oligonucleotide probes for flow cytometric identification of microorganisms. Cytometry **14**: 136–143. doi:10.1002/cyto.990140205

Wemheuer, B., S. Güllert, S. Billerbeck, H.-A. Giebel, S. Voget, M. Simon, and R. Daniel. 2014. Impact of a phytoplankton bloom on the diversity of the active bacterial community in the southern North Sea as revealed by metatranscriptomic approaches. FEMS Microbiology Ecology **87**: 378–389. doi:10.1111/1574-6941.12230

Wemheuer, B., F. Wemheuer, J. Hollensteiner, F.-D. Meyer, S. Voget, and R. Daniel. 2015. The green impact: bacterioplankton response toward a phytoplankton spring bloom in the southern North Sea assessed by comparative metagenomic and metatranscriptomic approaches. Frontiers in Microbiology **6**.

Winter, C., M. M. Moeseneder, and G. J. Herndl. 2001. Impact of UV Radiation on Bacterioplankton Community Composition. Applied and Environmental Microbiology **67**: 665–672. doi:10.1128/AEM.67.2.665-672.2001

Wurl, O., W. Ekau, W. M. Landing, and C. J. Zappa. 2017. Sea surface microlayer in a changing ocean – A perspective J.W. Deming and J. Bowman [eds.]. Elementa: Science of the Anthropocene **5**: 31. doi:10.1525/elementa.228

Wurl, O., E. Wurl, L. Miller, K. Johnson, and S. Vagle. 2011. Formation and global distribution of sea-surface microlayers. Biogeosciences **8**: 121–135. doi:10.5194/bg-8-121-2011